PAPER

Check for updates

cis-1 Isomers of tethered bismethano[70]fullerene as electron acceptors in organic photovoltaics†

Tomokazu Umeyama, [ID] *[a] Shogo Takahara,[a] Sho Shibata,[a] Kensho Igarashi,[a] Tomohiro Higashino, [ID] [a] Kenji Mishima,[b] Koichi Yamashita[b] and Hiroshi Imahori [ID] *[ac]

Isomer-controlled [70]fullerene bis-adducts can achieve high performance as electron-acceptors in organic photovoltaics (OPVs) because of their stronger absorption intensities than [60]fullerene derivatives, higher LUMO energy levels than mono-adducts, and less structural and energetic disorder than random isomer mixtures. Especially, attractive are *cis*-1 isomers that have the closest proximity of addends owing to their plausible more regular close packed structure. In this study, propylene-tethered *cis*-1 bismethano[70]fullerene with two methyl, ethyl, phenyl, or thienyl groups were rationally designed and prepared for the first time to investigate the OPV performances with an amorphous conjugated polymer donor (PCDTBT). The *cis*-1 products were found to be a mixture of two regioisomers, α-1-α and α-1-β as major and minor components, respectively. Among them, the *cis*-1 product with two ethyl groups (Et₂-*cis*-1-[70]PBC) showed the highest OPV performance, encouraging us to isolate its α-1-α isomer (Et₂-α-1-α-[70]PBC) by high-performance liquid chromatography. OPV devices based on Et₂-*cis*-1-[70]PBC and Et₂-α-1-α-[70]PBC with PCDTBT showed open-circuit voltages of 0.844 V and 0.864 V, respectively, which were higher than that of a device with typical [70]fullerene mono-adduct, [70]PCBM (0.831 V) with a lower LUMO level. However, the short-circuit current densities and resultant power conversion efficiencies of the devices with Et₂-*cis*-1-[70]PBC (9.24 mA cm⁻², 4.60%) and Et₂-α-1-α-[70]PBC (6.35 mA cm⁻², 3.25%) were lower than those of the device with [70]PCBM (10.8 mA cm⁻², 5.8%) due to their inferior charge collection efficiencies. The results obtained here reveal that *cis*-1 [70]fullerene bis-adducts do not guarantee better OPV performance and that further optimization of the substituent structures is necessary.

[a]Department of Molecular Engineering, Graduate School of Engineering, Kyoto University, Nishikyo-ku, Kyoto 615-8510, Japan

[b]Department of Chemical System Engineering, School of Engineering, The University of Tokyo, 7-3-1, Hongo, Bunkyo-ku, Tokyo 113-8656, Japan

[c]Institute for Integrated Cell-Material Sciences (WPI-iCeMS), Kyoto University, Sakyo-ku, Kyoto 606-8501, Japan. E-mail: umeyama@scl.kyoto-u.ac.jp; imahori@scl.kyoto-u.ac.jp; Fax: +81-75-383-2571; Tel: +81-75-383-2568; +81-75-383-2566

† Electronic supplementary information (ESI) available. See DOI: 10.1039/c8ra02896f

Introduction

Organic photovoltaic (OPV) devices have attracted scientific and industrial attention due to their advantages of low cost, light-weight, flexibility, and solution processing.[1–5] The photoactive layer generally comprises a blend film with a bulk hetero-junction (BHJ) structure of electron-donating conjugated polymers and electron-accepting organic semiconductors. Fullerene derivatives have been widely utilized as electron-acceptors[5] because of their reversible reduction behaviors, outstanding electron affinities, and excellent electron-transporting properties originating from their small reorganization energies of electron transfer,[6] whereas non-fullerene electron acceptors,

exhibiting high power conversion efficiencies (PCEs), have recently emerged as alternatives.[7–10]

PCEs of OPV devices are determined by the product of short-circuit current density (J_{SC}), open-circuit voltage (V_{OC}), and fill factor (FF); therefore, all three factors should be increased to achieve a high PCE.[1,2] [70]Fullerene derivatives such as [6,6]-phenyl-C_{71}-butyric acid methyl ester ([70]PCBM) are preferentially employed in high-performance OPVs instead of [60]fullerene derivatives owing to the former's better light-harvesting ability in the visible region, which improves J_{SC}.[11,12] The higher solubility of [70]fullerene derivatives than those of [60]fullerene derivatives is beneficial for device fabrication processes. Another strategy for developing high-performance acceptors is the use of fullerene bis-adducts.[1,13] By increasing the number of addends from one to two, the degree of π-conjugation is reduced and the energy level of the lowest unoccupied molecular orbital (LUMO) is raised. Since V_{OC} is generally proportional to the energy difference between the LUMO of the electron-acceptor and the highest occupied molecular orbital (HOMO) of the electron-donor,[1,2] the rise in the LUMO energy of electron-acceptors improves V_{OC}. Bis-[6,6]-phenyl-C_{61}-butyric acid methyl ester (bis-[60]PCBM),[14] indene-

C_{60} bis-adduct ([60]ICBA),[15] and indene-C_{70} bis-adduct ([70] ICBA)[12] are successful examples of fullerene bis-adduct acceptors in OPVs. However, even if both the addends are identical and symmetric and additions are limited to occur at [6,6]-bonds, there are 8 possible regioisomers of [60]fullerene bis-adducts. Furthermore, [70]fullerene bis-adducts have 38 possible regioisomers[16] because a [70]fullerene cage has four different types of non-equivalent [6,6]-bonds, i.e., α-, β-, γ-, and δ-type bonds (Fig. 1a),[17–20] although the differences in reactivity (α > β > γ > δ) and steric hindrance reduce the number of bis-adduct regioisomers actually obtained.[21,22] Due to different structural and electronic properties of each regioisomer, disorders in molecular packing and energy levels are found in BHJ films while using the regioisomer mixture, which may deteriorate J_{SC} and FF of BHJ OPV devices.[12,14,15] Therefore, the development of regioisomer-controlled acceptors is effective for improving OPV device performance, which has been proven by various examples of regioisomer-free [60]fullerene bis-adducts.[23–35]

Regioisomer-controlled [70]fullerene bis-adducts are expected to be high-performance acceptors for BHJ OPVs, as is evident from the above argument. However, the number of reports that demonstrate this is limited[36–39] compared to the case of regioisomer-free [60]fullerene bis-adducts.[23–35] This is due to the synthetic difficulty originating from the formation of a complicated mixture containing multiple regioisomers of [70] fullerene bis-adducts. In a pioneering work by Wong and coworkers,[37] a single regioisomer of [70]ICBA, i.e., α-7-α′ isomer (Fig. 1b),[40] in which two indene units were attached at α-bonds belonging to different hemispheres with an angle of "2 o'clock", was carefully isolated from the regioisomer mixture by high-performance liquid chromatography (HPLC). The regioisomer pure α-7-α′-[70]ICBA exhibited better OPV device performance than the [70]ICBA regioisomer mixture. We devised tether-directed bis-functionalization of [70]fullerene with an ethylene-bridged indene dimer (1,2-bis(3-indenyl)ethane, BIE) as reactant to selectively obtain a relatively close substituent pattern, i.e., cis-2 (α-2-α) type isomer (Fig. 1b),[40] in which two indene units were attached at α-bonds of hexagons next to each other.[38] Note here that steric hindrance between the addends would inhibit the formation of such a close substitution pattern

if the tether-directed effect was absent.[23,27] The OPV based on BIE–[70]fullerene bis-adduct isomer with cis-2 configuration, cis-2-[70]BIEC and poly(3-hexylthiophene) showed a remarkable PCE of 4.2%, which was higher than those with the regioisomer mixture of BIE–[70]fullerene bis-adduct (2.2%), BIE–[70] fullerene mono-adduct (2.2%), BIE–[60]fullerene bis-adduct isomer with cis-2 configuration (2.8%), and even [70]PCBM (3.8%). This result has encouraged us to use cis-1 isomers of [70] fullerene bis-adducts having the closest proximity of two addends on a [70]fullerene cage because of their plausible regular close packing in the BHJ structure with conjugated polymers.

Recently, Echegoyen et al. succeeded in synthesizing a bis-methano[70]fullerene derivative with cis-1 configuration, i.e., attached to [6,6]-bonds in the same hexagon, through a tether-directed remote functionalization method.[16,41] They conducted a reaction between [70]fullerene and 1,3-dibenzoylpropane bis-p-toluenesulfonyl hydrazone (Ph₂-PBTH) as addend precursor, yielding propylene-tethered cis-1 bismethano[70]fullerene with two phenyl groups (Ph₂-cis-1-[70]PBC, Scheme 1). Ph₂-cis-1-PBC was further separated to α-1-α and α-1-β isomers (Fig. 1b) by preparative thin layer chromatography and their structures were fully characterized. However, the photovoltaic properties of these tethered bis-adducts of [70]fullerene were not evaluated. In this study, for the first time, we utilized propylene-tethered cis-1 bismethano[70]fullerene as an electron-accepting material in OPV devices. Bis-adducts with methyl, ethyl, phenyl and thienyl groups (Scheme 1) were designed as substituents based on theoretical calculations on the degree of molecular packing (i.e., packing density) and prepared for investigating the substituent effects on film structures and photovoltaic properties of blend films with an amorphous conjugated polymer donor, poly[N-9′-heptadecanyl-2,7-carbazole-alt-5,5-(4′,7′-di-2-thienyl-2′,1′,3′-benzothiadiazole)] (PCDTBT).[42,43]

Results and discussion

Densely packed fullerenes in blend films are advantageous over loosely packed ones because the former provides films with higher electron mobilities than the latter.[17] This helps achieve higher performance for fullerene acceptor-based OPV devices.
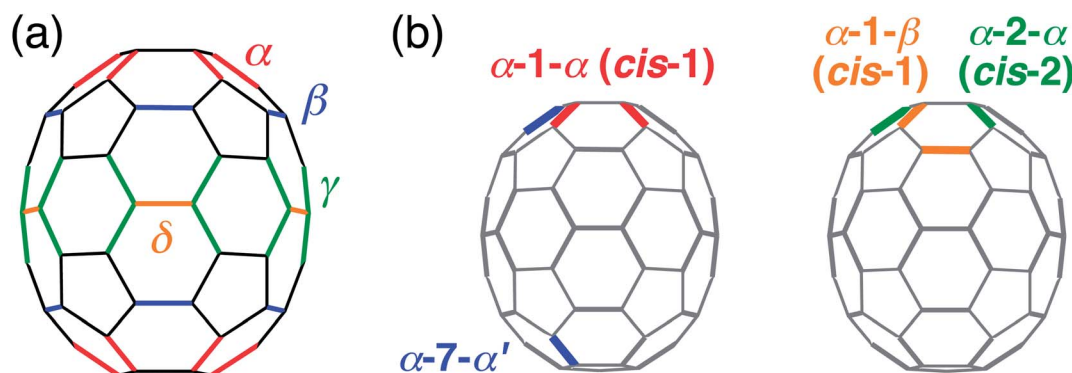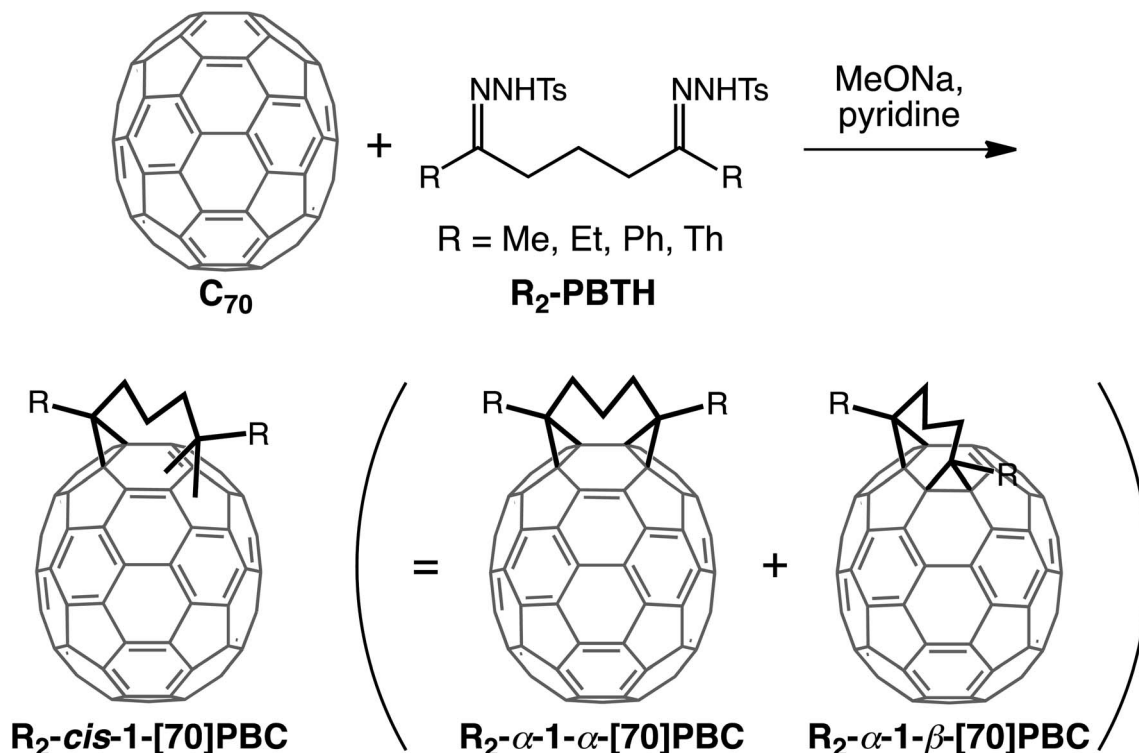

Fig. 1 (a) Structure of [70]fullerene. α-, β-, γ-, and δ-type [6,6]-bonds are represented by red, blue, green and orange lines. (b) Examples of names for [70]fullerene bis-adduct patterns.

Scheme 1 Synthesis of R_2-*cis*-1-[70]PBC.

In addition, well-packed fullerenes at the donor–acceptor interface facilitate charge dissociation.[44,45] Therefore, optimized structures for solid systems of propylene-tethered bismethano [70]fullerenes with various substituents, *i.e.*, R_2-α-1-α-[70]PBC (R = methyl (Me), ethyl (Et), i-propyl (iPr), cyano (CN), phenyl (Ph), thienyl (Th), and pyridyl (Py)) (Fig. S1†), were calculated using periodic boundary conditions on MOPAC to sort the suitable substituents. Volumes of one molecule (V_0) and of a unit cell (V) were obtained based on the optimized structures (Table 1 and Fig. S2†). The unit cells included four molecules and the degree of molecular packing was defined as $4V_0/V$.[46] Among alkyl-substituted bis-adducts (R = Me, Et, iPr), the ethyl-substituted one showed the smallest V (5170 Å^3) and highest

degree of packing (0.712), suggesting high potential as an electron-accepting material in OPV devices. The packing degree of Et_2-α-1-α-[70]PBC was higher than that of [70]PCBM (0.683, Table 1). The packing degree of iPr_2-α-1-α-[70]PBC (0.667) was slightly higher than that of Me_2-α-1-α-[70]PBC (0.643). However, the insulating alkyl chain of iPr_2-α-1-α-[70]PBC was longer than that of Me_2-α-1-α-[70]PBC. Overall, Et_2-α-1-α-[70]PBC and Me_2-α-1-α-[70]PBC were chosen as synthetic targets. In propylene-tethered bismethano[70]fullerenes with aromatic substituent groups (R = Ph, Th, Py), the phenyl- and thienyl-substituted ones possessed higher packing degrees (0.660 and 0.670, respectively) than the pyridyl one (0.639). Thus, Ph_2-α-1-α-[70] PBC and Th_2-α-1-α-[70]PBC were selected. Although CN_2-α-1-α-[70]PBC exhibited a higher packing degree (0.672), synthetic difficulty impeded the attempt.

Propylene-tethered *cis*-1 bismethano[70]fullerene with methyl, ethyl, or thienyl groups (R_2-*cis*-1-[70]PBC (R = Me, Et, Th)) was synthesized using the method used for Ph_2-*cis*-1-[70] PBC (Scheme 1).[16] The reaction between [70]fullerene and addend precursor, 1,3-dicarbonylpropane bis-*p*-toluenesulfonyl hydrazone (R_2-PBTH) yielded a crude product, which was purified by silica gel chromatography using CS_2 as eluent and then preparative HPLC with a Buckyprep column using toluene as eluent. Only three [70]fullerene-based fractions, *i.e.*, unreacted pristine [70]fullerene, R_2-*cis*-1-[70]PBC, and multiple adducts, were eluted during HPLC. The overall yields of R_2-*cis*-1-[70]PBC with Me, Et, and Th groups were 5.2%, 28%, and 17%, respectively. Analyses of the HPLC traces revealed that the *cis*-1 products consisted of two regioisomers, α-1-α as the major

Table 1 Volumes of one molecule (V_0), volumes of a unit cell (V), and packing degrees

Fullerene	V_0 (bohr^3 per molecule)[a]	V (Å^3)[b]	Packing degree[c]
Me_2-α-1-α-[70]PBC	5660	5220	0.643
Et_2-α-1-α-[70]PBC	6210	5170	0.712
iPr_2-α-1-α-[70]PBC	6240	5550	0.667
CN_2-α-1-α-[70]PBC	5890	5200	0.672
Ph_2-α-1-α-[70]PBC	6870	6170	0.660
Th_2-α-1-α-[70]PBC	6230	5520	0.670
Py_2-α-1-α-[70]PBC	7400	6860	0.639
[70]PCBM	6190	5380	0.683

[a] Estimated by DFT at RB3LYP/6-31G(d) level. [b] Calculated after optimizations of fullerene solid systems under periodic boundary conditions at PM6-D3 based on MOPAC. All unit cells contain 4 molecules. [c] Defined as $4V_0/V$.

Table 2 Composition ratios, solubilities, and LUMO energy levels of fullerenes

Fullerene	Ratio of α-1-α isomer[a] (%)	Solubility[b] (g mL^{-1})	LUMO[c] (eV)
Me$_2$-*cis*-1-[70]PBC	67	3.6	—[d]
Et$_2$-*cis*-1-[70]PBC	78	11.6	−3.67
Ph$_2$-*cis*-1-[70]PBC	68	13.8	−3.67
Th$_2$-*cis*-1-[70]PBC	60	5.8	−3.66
Et$_2$-α-1-α-[70]PBC	>99	6.2	−3.65
[70]PCBM	—	62.9	−3.70

[a] Estimated by the peak area ratio in HPLC traces. [b] Measured in ODCB at room temperature. [c] LUMO = $-e(4.80 + E_1)$ eV; E_1 is the first reduction potential of fullerenes *vs.* ferrocene/ferrocenium (Fc/Fc$^+$) couple. [d] Not determined due to the low solubility.

component (60–78%) and α-1-β as the minor one (Table 2 and Fig. S3, ESI†). This was consistent with the previous result for Ph$_2$-*cis*-1-[70]PBC (α-1-α : α-1-β = 78 : 22).[16,47] Owing to the difference in the reactivities of [6,6]-bonds in the [70]fullerene cage (α > β > γ > δ), the first reaction occurred mainly at an α-bond. In addition, the short propylene chain limited the second reaction site to the α- or β-bond on the same hexagon. The structures of R$_2$-*cis*-1-[70]PBC (R = Me, Et, Th) were characterized by ^{1}H-NMR and high-resolution mass spectrometry (Experimental section). UV-vis absorption spectra of R$_2$-*cis*-1-[70]PBC (R = Me, Et, Ph, Th) showed similar absorption shapes and intensities as those of [70]PCBM (Fig. S4, ESI†).

Solubility tests of R$_2$-*cis*-1-[70]PBC (R = Me, Et, Ph, Th) in a standard organic solvent for OPV device fabrication, *i.e.*, *o*-dichlorobenzene (ODCB), were carried out at room temperature (Table 2). The solubility of Me$_2$-*cis*-1-[70]PBC (3.6 g mL^{-1}) was found to be unsatisfactory for film formation by the spin-coating technique. Considering the low solubility and theoretically-predicted undesirable loose packing (*vide supra*), the properties of Me$_2$-*cis*-1-[70]PBC were not examined subsequently. The bis-adduct with thienyl groups, Th$_2$-*cis*-1-[70]PBC, exhibited solubility (5.8 mg mL^{-1}) somewhat being higher than that of Me$_2$-*cis*-1-[70]PBC and was used for OPV device fabrication (*vide infra*). Other bis-adducts, Et$_2$-*cis*-1-[70]PBC and Ph$_2$-*cis*-1-[70]PBC, possessed solubilities (11.6 and 13.8 mg mL^{-1}, respectively) sufficient for solution processes, whereas they were much lower than that of a widely used [70]fullerene mono-adduct acceptor, [70]PCBM (62.9 mg mL^{-1}).

Electrochemical properties of R$_2$-*cis*-1-[70]PBC (R = Et, Ph, Th) containing α-1-α (60–78%) and α-1-β isomers were evaluated by cyclic voltammetry (CV) and differential pulse voltammetry (DPV) measurements (Fig. S5, ESI†). The LUMO energy levels determined from the electrochemical data are listed in Table 2 together with that of [70]PCBM. The LUMO levels of R$_2$-*cis*-1-[70]PBC were 30–40 mV higher than that of [70]PCBM, which was desirable for photovoltaic application, improving V_{OC}.[1,2] To gain insight into the electronic structures of R$_2$-*cis*-1-[70]PBC, we performed DFT calculations of α-1-α isomers using the RB3LYP/6-31G(d) model. LUMO levels were obtained after geometry optimization, as illustrated in Fig. 2. The theoretical LUMO levels of R$_2$-α-1-α-[70]PBC (R = Et, Ph, Th) were similar (−2.90, −2.87, and −2.90 V, respectively) and significantly higher than that of [70]PCBM (−3.06 V), which agreed with those obtained from electrochemical measurements (Table 2). The orbital

distributions of the HOMOs and LUMOs of the fullerene bis-adducts were primarily found only in the [70]fullerene cage and delocalized throughout the entire cage (Fig. 2). Theoretical calculations of R$_2$-α-1-β-[70]PBC contained in R$_2$-*cis*-1-[70]PBC as minor component (22–40%) showed similar LUMO energy levels and orbital distributions as those of R$_2$-α-1-α-[70]PBC (Fig. S6, ESI†).

To investigate the photovoltaic properties of R$_2$-*cis*-1-[70]PBC (R = Et, Ph, Th) containing α-1-α and α-1-β isomers as major and minor components, OPV devices with the ITO/PEDOT:PSS/PCDTBT : fullerene/TiO$_x$/Al configuration were fabricated. The detailed device fabrication process is described in the Experimental section. The average current density–voltage characteristics and photovoltaic parameters are shown in Fig. 3a and Table 3, respectively. Since the solubility of Th$_2$-*cis*-1-[70]PBC in ODCB was lower than those of Et$_2$-*cis*-1-[70]PBC and Ph$_2$-*cis*-1-[70]PBC (Table 2), the optimized weight ratio of fullerene derivative in a mixed solution with PCDTBT was lower in PCDTBT : Th$_2$-*cis*-1-[70]PBC ([PCDTBT] : [fullerene] = 1 : 1 (w/
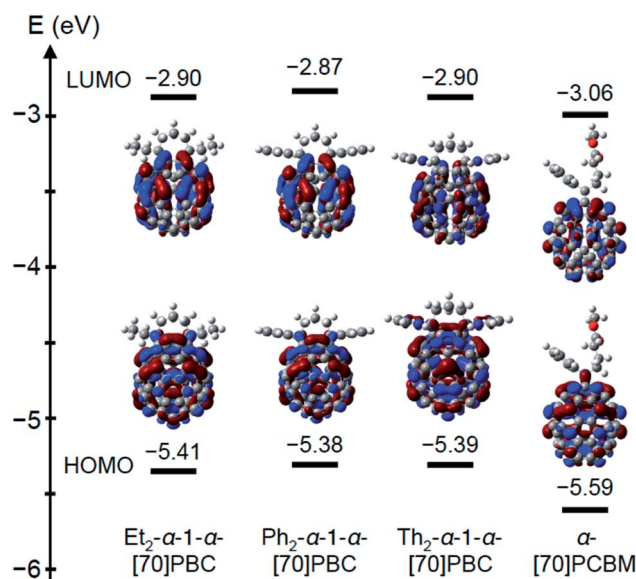

Fig. 2 Optimized geometries, HOMO/LUMO orbital distributions, and energy levels of Et$_2$-α-1-α-[70]PBC, Ph$_2$-α-1-α-[70]PBC, Th$_2$-α-1-α-[70]PBC, and α-isomer of [70]PCBM by DFT calculations using RB3LYP/6-31G(d) model.
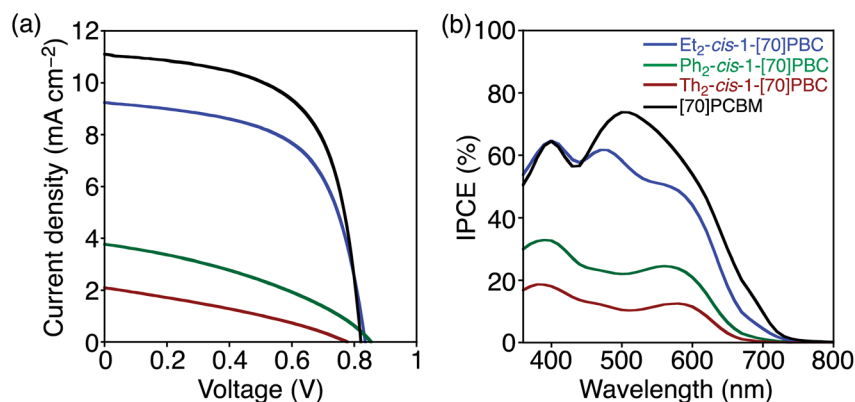
Fig. 3 (a) Current density–voltage curves and (b) photocurrent action spectra of OPV devices based on PCDTBT : Et$_2$-*cis*-1-[70]PBC (blue), PCDTBT : Ph$_2$-*cis*-1-[70]PBC (green), PCDTBT : Th$_2$-*cis*-1-[70]PBC (brown), and PCDTBT : [70]PCBM (black). The convolution of the spectral response in (b) with the photon flux of the AM 1.5G spectrum provided the estimated J_{SC} values of 8.82, 3.85, 1.98, and 10.8 mA cm^{-2}, respectively.

w)) than in PCDTBT : Et$_2$-*cis*-1-[70]PBC and PCDTBT : Ph$_2$-*cis*-1-[70]PBC (1 : 3 (w/w)) (Table 3).

The OPV device with Et$_2$-*cis*-1-[70]PBC revealed a significantly higher PCE of 4.60% than those with Ph$_2$-*cis*-1-[70]PBC (1.20%) and Th$_2$-*cis*-1-[70]PBC (0.59%) (Table 3). J_{SC} (3.81 and 2.13 mA cm^{-2}) and FF (0.364 and 0.327) of the devices with Ph$_2$-*cis*-1-[70] PBC and Th$_2$-*cis*-1-[70]PBC were remarkably lower than those of the Et$_2$-*cis*-1-[70]PBC-based device (9.24 mA cm^{-2} and 0.590). Reflecting the inferior J_{SC} values, the incident photon-to-current efficiencies (IPCEs) of devices with Ph$_2$-*cis*-1-[70]PBC and Th$_2$-*cis*-1-[70]PBC were significantly lower than those of the Et$_2$-*cis*-1-[70]PBC-based device over the entire visible region (Fig. 3b). Although PCDTBT : Et$_2$-*cis*-1-[70]PBC film exhibited higher absorption than PCDTBT : Ph$_2$-*cis*-1-[70]PBC and PCDTBT : Th$_2$-*cis*-1-[70]PBC in the region 430–530 nm (Fig. S7, ESI†), the difference in absorption intensity could not explain the significant difference in the IPCE values. Additionally, X-ray diffraction (XRD) measurements of all blend films displayed no significant signals, reflecting the amorphous nature of PCDTBT.

To search for a reason regarding poor OPV performances of the devices with Ph$_2$-*cis*-1-[70]PBC and Th$_2$-*cis*-1-[70]PBC, the blend film structures of photoactive layers were examined with an optical microscope. As shown in Fig. 4, aggregates with sizes of tens of micrometers were formed in PCDTBT : Ph$_2$-*cis*-1-[70] PBC and PCDTBT : Th$_2$-*cis*-1-[70]PBC. Similar large aggregates were absent in PCDTBT : Et$_2$-*cis*-1-[70]PBC, suggesting that the aggregates did not consist of PCDTBT but fullerenes in the blend films. Atomic force microscopy (AFM) visualized that the film surface roughnesses of PCDTBT : Ph$_2$-*cis*-1-[70]PBC and PCDTBT : Th$_2$-*cis*-1-[70]PBC (rms = 2.3 and 1.9 nm, respectively) at sites other than the aggregate were much larger than that of PCDTBT : Et$_2$-*cis*-1-[70]PBC (rms = 0.59 nm) (Fig. S8, ESI†). These results suggested that Ph$_2$-*cis*-1-[70]PBC and Th$_2$-*cis*-1-[70] PBC had strong cohesive natures even in the blend film with amorphous PCDTBT. Bicontinuous network structures of donor and acceptor domains were poorly formed in PCDTBT : Ph$_2$-*cis*-1-[70]PBC and PCDTBT : Th$_2$-*cis*-1-[70]PBC, resulting in inferior J_{SC} and FF values.

To investigate the diffusion efficiency of excitons generated in the polymer domain to the polymer–fullerene interface, we measured the steady-state photoluminescences of the blend films (Fig. S9, ESI†). The emission from PCDTBT was quenched efficiently (>98%) in PCDTBT : Et$_2$-*cis*-1-[70]PBC, PCDTBT : Ph$_2$-

Table 3   OPV device parameters,[a] electron mobilities (μ_e),[b] thicknesses, and surface roughnesses (rms)[c] of PCDTBT : fullerene films

Fullerene	[PCDTBT] : [fullerene] (w/w)	J_{SC} (mA cm^{-2})	V_{OC} (V)	FF	PCE (%)	Thickness (nm)	μ_e (10^{-4} cm^2 V^{-1} s^{-1})	rms (nm)
Et$_2$-*cis*-1-[70] PBC	1 : 3	9.24 ± 0.09	0.844 ± 0.005	0.590 ± 0.006	4.60 ± 0.05	75	0.59	0.59
Ph$_2$-*cis*-1-[70] PBC	1 : 3	3.81 ± 0.07	0.866 ± 0.006	0.364 ± 0.004	1.20 ± 0.03	57[d]	—[e]	2.3
Th$_2$-*cis*-1-[70] PBC	1 : 1	2.13 ± 0.08	0.787 ± 0.002	0.327 ± 0.003	0.59 ± 0.03	50[d]	—[e]	1.9
Et$_2$-α-1-α-[70] PBC	1 : 2	6.35 ± 0.04	0.864 ± 0.005	0.593 ± 0.005	3.25 ± 0.06	52[d]	0.51	0.78
[70]PCBM	1 : 4	10.8 ± 0.06	0.831 ± 0.004	0.618 ± 0.003	5.55 ± 0.05	91	6.9	0.35

[a] The data represent the average values with standard deviations from ten independent devices. [b] Measured by SCLC. [c] Measured by AFM. [d] Film thicknesses at sites without fullerene aggregates. [e] Not determined because the inhomogeneous film thickness due to the large aggregate formation hampered the accurate mobility estimations.
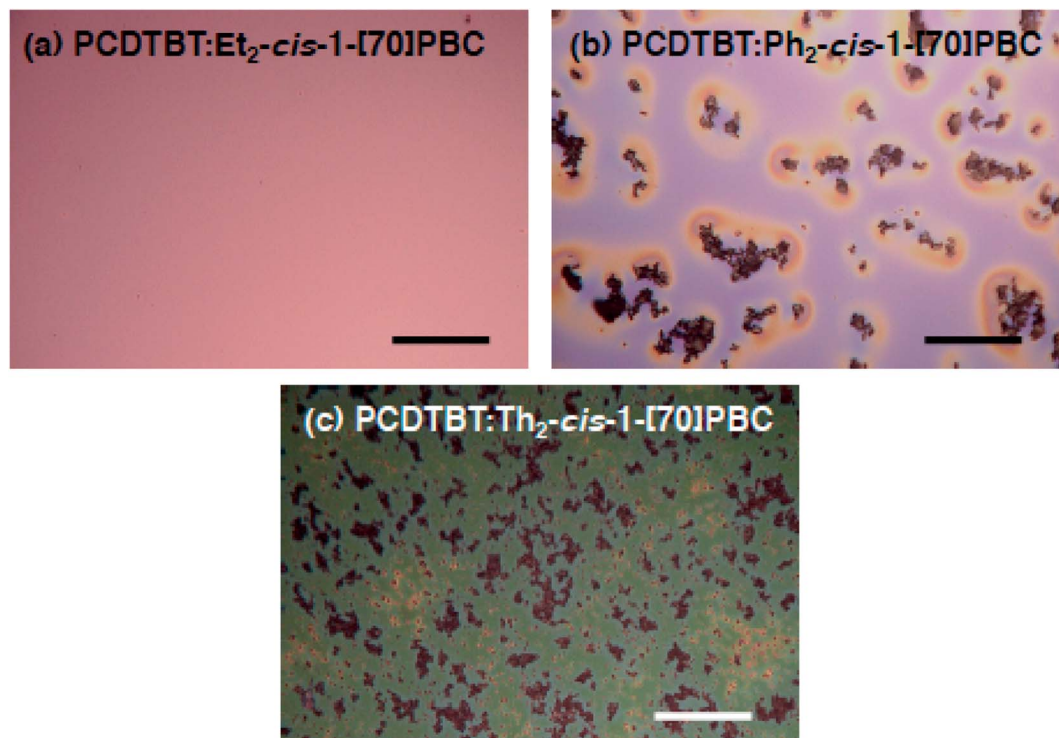
Fig. 4 Optical microscopy images of (a) PCDTBT : Et$_2$-*cis*-1-[70]PBC, (b) PCDTBT : Ph$_2$-*cis*-1-[70]PBC, and (c) PCDTBT : Th$_2$-*cis*-1-[70]PBC on ITO/PEDOT:PSS substrates. Scale bars represent 50 μm.

cis-1-[70]PBC, and PCDTBT : Th$_2$-*cis*-1-[70]PBC. This result suggested that Ph$_2$-*cis*-1-[70]PBC and Th$_2$-*cis*-1-[70]PBC molecules also existed outside the large aggregates and that most of the excitons generated by polymer absorption were quenched by fullerene molecules scattered across the polymer domain. However, such quenching did not lead to efficient photocurrent generation because of poor formation of an effective electron-transporting pathway to the electrode.

As expected, V_{OC} of the OPV with Et$_2$-*cis*-1-[70]PBC (0.844 V) was slightly higher than that with a prevalent high-performance [70]fullerene acceptor, [70]PCBM (0.831 V) (Table 3), as the result of the elevated LUMO level of Et$_2$-*cis*-1-[70]PBC by bis-functionalization. However, J_{SC} and FF of the PCDTBT : Et$_2$-*cis*-1-[70]PBC-based device (9.24 mA cm^{-2} and 0.590) were slightly lower than those of the PCDTBT : [70]PCBM-based one (10.8 mA cm^{-2} and 0.618), irrespective of the comparable light-harvesting efficiency (Fig. S7†). The lower J_{SC} and FF led to the inferior PCE of PCDTBT : Et$_2$-*cis*-1-[70]PBC (4.60%) relative to that of PCDTBT : [70]PCBM (5.55%). The smoother film surface of PCDTBT : [70]PCBM (rms = 0.35 nm) than that of PCDTBT : Et$_2$-*cis*-1-[70]PBC (rms = 0.59 nm) indicated the formation of a more suitable bicontinuous donor–acceptor network structure in PCDTBT : [70]PCBM (Fig. S10, ESI†). More importantly, the electron mobility of PCDTBT : Et$_2$-*cis*-1-[70]PBC (5.9 × 10^{-5} cm^2 V^{-1} s^{-1}) estimated by space-charge-limited current (SCLC) measurement was much lower than that of PCDTBT : [70]PCBM (6.9 × 10^{-4} cm^2 V^{-1} s^{-1}) (Table 3). The plausible lower charge collection efficiency of PCDTBT : Et$_2$-*cis*-1-[70]PBC than PCDTBT : [70]PCBM as a consequence of the

difference in the electron mobilities resulted in the inferior OPV device performance.

The lower OPV performances of devices with R$_2$-*cis*-1-[70]PBC (R = Et, Ph, Th) than that with [70]PCBM might be due to inhomogeneity of R$_2$-*cis*-1-[70]PBC containing two regioisomers, *i.e.*, α-1-α and α-1-β. Disorders of molecular packing structures and electronic properties caused by regioisomer inhomogeneity may decrease electron mobility in fullerene domains. To shed light into the regioisomer effect on film structure and OPV performance, the major α-1-α isomer was further isolated from the Et$_2$-*cis*-1-[70]PBC isomer mixture, which had showed the highest PCE among the R$_2$-*cis*-1-[70]PBC isomer mixtures (R = Et, Ph, Th), using preparative HPLC technique with a 5PBB column (Fig. S11(a), ESI†). Collection of the minor α-1-β isomer could not be conducted because of the low composition ratio (α-1-α : α-1-β = 78 : 22, Table 2) in Et$_2$-*cis*-1-[70]PBC that made it difficult to obtain sufficient amount of the α-1-β isomer for OPV device fabrication. The purity of the isolated α-1-α isomer sample (denoted as Et$_2$-α-1-α-[70]PBC) was estimated by HPLC trace and found to be >99% (Fig. S11(b), ESI†).[48] The solubility test in ODCB at room temperature revealed that Et$_2$-α-1-α-[70]PBC possessed lower solubility (6.2 g mL^{-1}) than Et$_2$-*cis*-1-[70]PBC (11.6 g mL^{-1}, Table 2). The highly symmetrical substitution structure of Et$_2$-α-1-α-[70]PBC (Scheme 1) may have enhanced its tendency to form insoluble aggregates. The optical and electrochemical properties of Et$_2$-α-1-α-[70]PBC were almost identical to those of Et$_2$-*cis*-1-[70]PBC, reflecting the high content of Et$_2$-α-1-α-[70]PBC in Et$_2$-*cis*-1-[70]PBC (Fig. S12, ESI†).

The OPV device based on PCDTBT : Et$_2$-α-1-α-[70]PBC blend film was fabricated by the same procedure as the device with
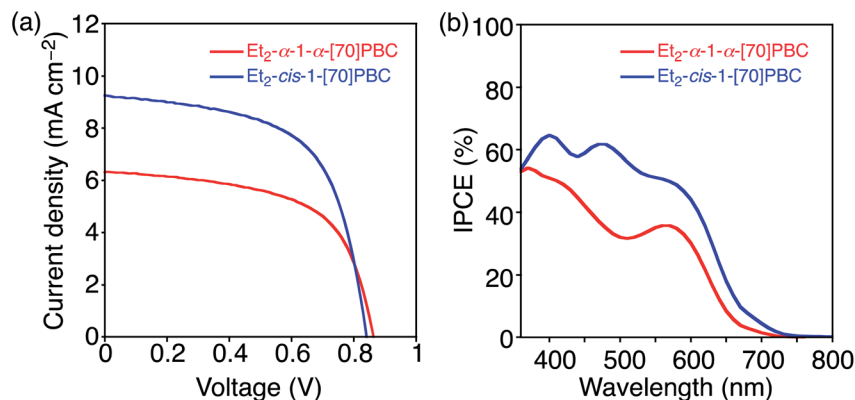
Fig. 5 (a) Current density−voltage curves and (b) photocurrent action spectra of OPV devices based on PCDTBT : Et$_2$-α-1-α-[70]PBC (red) and PCDTBT : Et$_2$-cis-1-[70]PBC (blue). The convolution of the spectral responses in (b) with the photon flux of the AM 1.5G spectrum provided the estimated J_{SC} values of 5.81 and 8.82 mA cm^{-2}, respectively.

PCDTBT : Et$_2$-cis-1-[70]PBC. The optimized weight ratio of fullerene in mixed solution with PCDTBT ([PCDTBT] : [Et$_2$-α-1-α-[70]PBC] = 1 : 2 (w/w)) was lower than PCDTBT : Et$_2$-cis-1-[70]PBC ([PCDTBT] : [Et$_2$-cis-1-[70]PBC] = 1 : 3 (w/w)) (Table 3) on account of the lower solubility of Et$_2$-α-1-α-[70]PBC. PCE of the OPV device with Et$_2$-α-1-α-[70]PBC was lower (3.25%) than that with Et$_2$-cis-1-[70]PBC (4.60%) (Fig. 5a and Table 3). Although V_{OC} and FF of the PCDTBT : Et$_2$-α-1-α-[70]PBC-based device (0.864 V and 0.593) were rather comparable to those of the PCDTBT : Et$_2$-cis-1-[70]PBC-based one (0.844 V and 0.590), J_{SC} of the former (6.35 mA cm^{-2}) was significantly lower than that of the latter (9.24 mA cm^{-2}). Consistently, IPCE of the former device was lower than that of the latter over the entire visible region (Fig. 5b). The slightly decreased absorption intensity of PCDTBT : Et$_2$-α-1-α-[70]PBC relative to that of PCDTBT : Et$_2$-cis-1-[70]PBC (Fig. S13(a), ESI†) was one of the reasons for inferior J_{SC}. The decrease in film thickness (Table 3) owing to the lower solubility of Et$_2$-α-1-α-[70]PBC was compatible with the decrease in the absorption intensity of PCDTBT : Et$_2$-α-1-α-[70]PBC. Although the efficient fluorescence quenching of PCDTBT in the blend film with Et$_2$-α-1-α-[70]PBC (Fig. S13(b)†) indicated high efficiency of exciton diffusion to the donor–acceptor interface, the optical microscopy image visualized the existence

of micrometer-sized aggregates in PCDTBT : Et$_2$-α-1-α-[70]PBC (Fig. 6). The film surface roughness of PCDTBT : Et$_2$-α-1-α-[70] PBC (rms = 0.78 nm) at sites other than the aggregate (Fig. S14, ESI†) was larger than that of PCDTBT : Et$_2$-cis-1-[70]PBC (rms = 0.59 nm) (Fig. S8, ESI†). These results indicate a poorly developed donor–acceptor bicontinuous network structure. Furthermore, despite the regioisomerically pure structure of Et$_2$-α-1-α-[70]PBC, the SCLC electron mobility of PCDTBT : Et$_2$-α-1-α-[70]PBC (5.1×10^{-5} cm^2 V^{-1} s^{-1}) was not improved relative to that of PCDTBT : Et$_2$-cis-1-[70]PBC (5.9×10^{-5} cm^2 V^{-1} s^{-1}) and was one order magnitude lower than that of PCDTBT : [70]PCBM (6.9×10^{-4} cm^2 V^{-1} s^{-1}) (Table 3). In sharp contrast with the BIE-[70]fullerene bis-adducts,[38] the regioisomer isolation of Et$_2$-α-1-α-[70]PBC from Et$_2$-cis-1-[70] PBC deteriorated the OPV device performance because of decrease in its solubility and higher tendency to form its aggregates.

Conclusion

cis-1 Bis-adduct fullerenes were utilized as electron acceptors in OPV devices for the first time. Propylene-tethered cis-1 bismethano[70]fullerenes (R$_2$-cis-1-[70]PBC) with two methyl, ethyl, phenyl, and thienyl groups were designed rationally and prepared to examine the substitution effect on the film structures and OPV performances of the blend films with an amorphous polymer, PCDTBT. R$_2$-cis-1-[70]PBC with ethyl groups (Et$_2$-cis-1-[70]PBC) showed the highest PCE (4.60%) as a result of good miscibility with PCDTBT. Owing to the elevated LUMO level, V_{OC} of the PCDTBT : Et$_2$-cis-1-[70]PBC-based device (0.844 V) was slightly higher than that of the PCDTBT : [70]PCBM-based one (0.831 V). The device performance of PCDTBT : Et$_2$-cis-1-[70]PBC was inferior to that of PCDTBT : [70]PCBM (PCE = 5.55%) due to lower electron mobility and charge collection efficiency. Isolation of the α-1-α isomer (Et$_2$-α-1-α-[70]PBC) from the corresponding isomer mixture, Et$_2$-cis-1-[70]PBC was also conducted, but PCE of the OPV device decreased (3.25%) despite removing the inhomogeneity of structure and electronic properties of the fullerene bis-adducts. The decreased solubility and enhanced aggregation
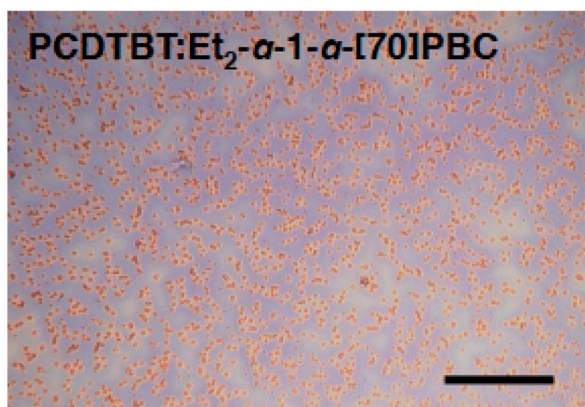

Fig. 6 Optical microscopy image of PCDTBT : Et$_2$-α-1-α-[70]PBC on ITO/PEDOT:PSS substrate. Scale bar represents 50 μm.

behavior of Et$_2$-α-1-α-[70]PBC relative to Et$_2$-cis-1-[70]PBC resulted in deteriorated OPV performance. These results obtained suggest that the optimization of substituent structure, considering their solubility, aggregation, and electron mobility as well as packing density, are indispensable for taking full advantage of regioisomerically pure cis-1 bis-adducts of [70]fullerene as electron-accepting materials. This model study provides important information for further research to modulate the fundamental properties of [70]fullerene bis-adduct materials, which will play a key role in making advance of OPV devices.

Experimental

Instruments

^{1}H NMR and ^{13}C NMR spectra were measured with a JEOL JNM-EX400 NMR spectrometer. High-resolution mass spectra were measured on a JEOL JMS-700 MStation spectrometer. Attenuated total reflectance (ATR) FT-IR spectra were recorded on a ThermoFisher Scientific Nicolet 6700 FT-IR. Purification of fullerene derivatives was conducted by Shimadzu Prominence Modular HPLC with Nacalai Tesque Buckyprep (20 × 250 mm); eluent, toluene; flow rate, 10 mL min^{-1}; temperature, 40 °C; detection, 330 nm. Regioisomer separation of Et$_2$-cis-1-[70]PBC was conducted by Shimadzu Prominence Modular HPLC with Nacalai Tesque Cosmosil 5PBB (20 × 250 mm); eluent, toluene; flow rate, 10 mL min^{-1}; temperature, 40 °C; detection, 330 nm. UV-vis absorption spectra were obtained on a Perkin Elmer Lambda 900 UV/vis/NIR spectrometer. Cyclic voltammetry (CV) and differential pulse voltammetry (DPV) measurements were performed using an ALS 630A electrochemical analyzer in an o-dichlorobenzene/acetonitrile mixture (v/v = 5 : 1) containing 0.1 M tetrabutylammonium hexafluorophosphate (Bu$_4$NPF$_6$) as a supporting electrolyte. Optical micrographs were recorded using KH-7700 (Hirox). Atomic force microscopy (AFM) analyses were carried out with an Asylum Technology MFP-3D-SA in the AC mode. X-ray diffraction (XRD) analyses of film samples were performed with a Rigaku SmartLab 9 kW using Cu Kα radiation. Samples for the X-ray measurements were prepared by spin-coating the polymer : fullerene solution on the glass substrate. Steady-state fluorescence spectra were recorded on a HORIBA NanoLog-TCSPC.

Photocurrent–voltage characteristics were measured by Keithley 2400 SourceMeter under a nitrogen atmosphere and simulated solar light (100 mW cm^{-2}, AM1.5) with OTENTO-SUN III solar simulator (Bunkoukeiki). Photocurrent action spectra were recorded with CEP-2000RR (Bunkoukeiki). Current–voltage characteristics of the electron- and hole-only devices for space-charge-limited current (SCLC) measurements were conducted using Keithley 2400 SourceMeter under a nitrogen atmosphere.

Materials

Ph$_2$-cis-1-[70]PBC and PCDTBT were prepared according to the reported procedure.[16,43] Nonane-3,7-dione,[49] heptane-2,6-dione,[50] and 1,5-di(thiophen-2-yl)pentane-1,5-dione[51] were prepared by the reaction between N^1,N^5-dimethoxy-N^1,N^5-

dimethylglutaramide and the corresponding Grignard reagent. C$_{70}$ (98.0%) and phenyl C$_{71}$-butyric acid methyl ester ([70]PCBM, >99.0%) were purchased from MTR Ltd. and American Dye Source, Inc, respectively. All other solvents and chemicals were of reagent-grade quality, purchased commercially, and used without further purification unless otherwise noted.

Synthesis

1,3-Dipropionylpropane bis-p-toluenesulfonyl hydrazone (Et$_2$-PBTH). In a 100 mL two-neck flask, a mixture of nonane-3,7-dione (1.40 g, 8.97 mmol) and p-toluenesulfonyl hydrazone (H$_2$NNHTs, 4.02 g, 21.1 mmol) in methanol (45 mL) was refluxed overnight. The mixture was evaporated and recrystallized from MeOH. The product as white solid (2.02 g, yield: 46%) was obtained. ^{1}H NMR (400 MHz, CDCl$_3$, ppm): δ 7.88 (d, 4H, J = 8.3 Hz); δ 7.30 (d, 4H, J = 8.3 Hz); δ 7.20 (br, 2H); δ 2.42 (s, 6H); δ 2.21–2.09 (m, 8H); δ 1.71 (m, 2H); δ 0.97 (t, 6H, J = 7.6 Hz). ^{13}C NMR (100 MHz, CDCl$_3$, ppm): δ 143.97, 135.37, 128.37, 125.97, 29.16, 27.98, 24.29, 21.70, 21.06, 12.02. IR (ATR, cm^{-1}): ν_{max} 3188, 2919, 2818, 1598, 1403, 1327, 1166, 1089, 1015, 926, 810, 666, 568. HRMS (ESI) m/z calcd for [C$_{23}$H$_{32}$N$_4$O$_4$S$_2$ − H]$^-$ 491.1792, found 491.1789. Melting point: 164–166 °C.

1,3-Diacetylpropane bis-p-toluenesulfonyl hydrazone (Me$_2$-PBTH). The target compound was synthesized by the same procedure for Et$_2$-PBTH using heptane-2,6-dione instead of nonane-3,7-dione. The product as white solid (0.68 g, yield: 16%) was obtained. ^{1}H NMR (400 MHz, CDCl$_3$, ppm): δ 7.81–7.66 (m, 4H); δ 7.38–7.19 (m, 6H); δ 2.47 (s, 6H); δ 2.42 (s, 6H); δ 2.05–1.71 (m, 6H). ^{13}C NMR (100 MHz, CDCl$_3$, ppm): δ 135.19, 130.70, 129.78, 128.09, 39.50, 29.16, 21.82, 18.58. IR (ATR, cm^{-1}): ν_{max} 3217, 2959, 1597, 1402, 1285, 1145, 1073, 1019, 922, 814, 668, 549. HRMS (APCI) m/z calcd for [C$_{21}$H$_{28}$N$_4$O$_4$S$_2$ + H]$^+$ 465.1625, found 465.1609. Melting point: 138–140 °C.

1,3-Dithenoylpropane bis-p-toluenesulfonyl hydrazone (Th$_2$-PBTH). The target compound was synthesized by the same procedure for Et$_2$-PBTH using 1,5-di(thiophen-2-yl)pentane-1,5-dione instead of nonane-3,7-dione. The product as pale yellow solid (1.00 g, yield: 76%) was obtained. ^{1}H NMR (400 MHz, CDCl$_3$, ppm): δ 8.23 (br, 2H); δ 7.80 (m, 4H); δ 7.19 (m, 6H); δ 6.96 (d, 2H, J = 3.9 Hz); δ 6.84 (t, 2H, J = 4.4 Hz); δ 2.53 (t, 2H, J = 8.3 Hz); δ 2.30 (m, 4H); δ 1.18 (s, 6H). ^{13}C NMR (100 MHz, CDCl$_3$, ppm): δ 151.35, 144.49, 141.67, 134.82, 129.74, 128.56, 128.37, 127.38, 126.79, 27.14, 22.50, 21.68. IR (ATR, cm^{-1}): ν_{max} 3216, 2965, 2924, 1598, 1434, 1391, 1338, 1163, 1086, 1040, 918, 812, 708, 666, 596. HRMS (ESI) m/z calcd for [C$_{27}$H$_{28}$N$_4$O$_4$S$_4$ + H]$^+$ 601.1066, found 601.1054. Melting point: 197–198 °C.

Et$_2$-cis-1-[70]PBC. In a dried 500 mL two-neck flask, C$_{70}$ (0.21 g, 0.25 mmol), anhydrous pyridine (0.61 mL), MeONa (0.13 g, 2.4 mmol), and Et$_2$-PBTH (0.13 g, 0.26 mmol) were dissolved in dry toluene (180 mL) and stirred at 70 °C for 2 days. The mixture was evaporated and short-passed by silica gel column chromatography using CS$_2$ as the eluent. The residue was subjected to preparative HPLC with Buckyprep column and the product as brown solid (0.068 g, yield: 28%) was obtained. Et$_2$-cis-1-[70]PBC consists of the α-1-α and α-1-β isomers with

the ratio of 78 : 22 (HPLC peak area ratio). ^{1}H NMR (400 MHz, *o*-dichlorobenzene-*d*$_4$, ppm): δ 2.55 (m, 6H); δ 2.49 (m, 6H); δ 2.27 (m, 4H); δ 2.27 (m, 4H); δ 1.95 (m, 16H); δ 1.79 (m, 1H); δ 1.57 (m, 1H); δ 1.16 (m, 1H); δ 1.02 (t, 21H, J = 7.4 Hz); δ 0.79 (t, 3H, J = 7.6 Hz). ^{13}C NMR (100 MHz, *o*-dichlorobenzene-*d*$_4$, ppm): δ 155.59, 152.03, 151.24, 151.10, 150.96, 150.72, 150.39, 149.50, 149.18, 148.96, 148.84, 148.45, 148.25, 148.07, 147.94, 147.72, 147.43, 147.16, 146.72, 146.22, 146.08, 145.94, 145.81, 145.51, 145.33, 144.58, 144.48, 144.22, 144.02, 143.81, 143.69, 143.45, 143.14, 142.96, 142.60, 142.30, 141.45, 141.33, 141.21, 140.85, 139.74, 139.32, 139.15, 138.83, 71.83, 69.40, 65.46, 36.68, 35.99, 34.47, 28.28, 27.08, 20.14, 19.48, 18.93, 12.69. IR (ATR, cm^{-1}): ν_{max} 3003, 2897, 1429, 1380, 867, 691, 677, 643, 594, 524, 510. HRMS (APCI) *m/z* calcd for $[C_{79}H_{16} - H]^+$ 961.1017, found 961.1009. Melting point: >300 °C.

Et$_2$-α-1-α-[70]PBC. Et$_2$-*cis*-1-[70]PBC (0.068 g) was subjected to preparative HPLC with 5PBB column and regioisomerically pure Et$_2$-α-1-α-[70]PBC as brown solid (0.058 g, yield: 85%) was obtained. ^{1}H NMR (400 MHz, *o*-dichlorobenzene-*d*$_4$, ppm): δ 2.56 (m, 2H); δ 2.47 (m, 2H); δ 1.94 (m, 4H); δ 1.12 (m, 2H); δ 1.02 (t, 6H, J = 7.4 Hz); ^{13}C NMR (100 MHz, *o*-dichlorobenzene-*d*$_4$, ppm): δ 155.58, 152.02, 151.22, 150.92, 150.71, 150.37, 149.10, 148.95, 148.36, 148.24, 148.06, 147.93, 147.71, 147.44, 147.15, 146.71, 146.25, 145.99, 145.50, 144.48, 144.01, 143.68, 143.44, 143.13, 142.90, 142.24, 141.44, 141.20, 140.79, 139.73, 139.30, 139.13, 138.82, 132.68, 71.72, 69.39, 34.40, 28.27, 27.06, 19.46, 12.67. IR (ATR, cm^{-1}): ν_{max} 3009, 2847, 1491, 1409, 894, 628, 604, 531, 518, 505. HRMS (APCI) *m/z* calcd for $[C_{79}H_{16} + H]^+$ 963.1168, found 963.1151. Melting point: >300 °C.

Me$_2$-*cis*-1-[70]PBC (R = Me). In a dried 200 mL two-neck flask, C$_{70}$ (0.20 g, 0.24 mmol), anhydrous pyridine (1.3 mL), MeONa (0.14 g, 2.5 mmol), and Me$_2$-PBTH (0.13 g, 0.28 mmol) were dissolved in anhydrous *o*-dichlorobenzene (80 mL) and stirred at 150 °C for 2 days. The mixture was evaporated and short-passed by silica gel column chromatography using CS$_2$ as the eluent. The residue was subjected to preparative HPLC with Buckyprep column and the product as brown solid (0.012 g, yield: 5.2%) was obtained. Me$_2$-*cis*-1-[70]PBC consists of the α-1-α and α-1-β isomers with the ratio of 67 : 33 (HPLC peak area ratio). ^{1}H NMR (400 MHz, CDCl$_3$, ppm): δ 2.13–1.96 (m, 6H); δ 1.81 (s, 6H). No clear signal was observed in ^{13}C NMR spectrum. IR (ATR, cm^{-1}): ν_{max} 2928, 2901, 1428, 1359, 1131, 671, 579. HRMS (ESI) *m/z* calcd for $[C_{77}H_{12} + H]^+$ 935.0861, found 935.0834. Melting point: >300 °C.

Th$_2$-*cis*-1-[70]PBC (R = Th). In a dried 500 mL two-neck flask, C$_{70}$ (0.20 g, 0.24 mmol), anhydrous pyridine (1.4 mL), MeONa (0.18 g, 3.3 mmol), and Th$_2$-PBTH (0.23 g, 0.38 mmol) were dissolved in dry toluene (200 mL) and stirred at 100 °C overnight. The mixture was evaporated and the residue was purified by silica gel column chromatography using CS$_2$ as the eluent. The product as brown solid (0.045 g, yield: 17%) was obtained. Th$_2$-*cis*-1-[70]PBC consists of the α-1-α and α-1-β isomers with the ratio of 60 : 40 (HPLC peak area ratio). ^{1}H NMR (400 MHz, CDCl$_3$/CS$_2$ (3/7), ppm): δ 7.44–7.42 (m, 2H); δ 7.34–7.29 (m, 5H); δ 7.23–7.20 (m, 1H); δ 7.12–7.06 (m, 1H); δ 7.01 (t, 3H, J = 4.4 Hz); δ 6.75–6.70 (m, 1H); δ 3.44–3.39 (m, 1H); δ 3.28–3.09 (m, 3H); δ 3.00–2.80 (m, 4H); δ 1.90–1.77 (m, 2H); δ 0.93–0.81 (m,

1H). No clear signal was observed in ^{13}C NMR spectrum. IR (ATR, cm^{-1}): ν_{max} 2920, 2854, 1430, 1232, 903, 731, 698, 645, 630, 585. HRMS(APCI) *m/z* calcd for $[C_{83}H_{12}S_2 + Cl]^-$ 1107.0074, found 1107.0063. Melting point: >300 °C.

Theoretical calculations

Geometry optimization, electronic structure calculations and molecular volume estimations for the fullerene compounds were performed using density functional theory (DFT) at the RB3LYP/6-31G(d) level. Calculations were carried out using the Gaussian 09 program.[52] All structures were fully optimized without any symmetry restriction. Optimized structures of fullerene derivatives in packed systems were calculated under periodic boundary conditions at PM6-D3 based on MOPAC. Degree of packing was calculated by Nv_0/V, where N is number of molecules in unit cell, v_0 is volume of a molecule, and V is volume of unit cell.[46]

Device fabrications

OPV devices were prepared on patterned indium tin oxide (ITO) substrates that were cleaned by ultra-sonication in deionized water, CHCl$_3$, acetone, and tetramethylammonium hydroxide aqueous solution for 15 min each, and then deionized water for 25 min, followed by 2-propanol and ethanol for 15 min each. They were subsequently dried under nitrogen flow, and treated in a UV–ozone cleaner for 25 min. A thin layer of poly(3,4-ethylenedioxythiophene):polystyrene sulfonate (PEDOT:PSS) was spin-coated on substrates at 1000 rpm for 60 s, followed by 4000 rpm for 10 s. The PEDOT:PSS layer was dried at 200 °C for 10 min, and then transferred into a glove box filled with dried N$_2$ gas to coat the active layer. A blended solution of PCDTBT and fullerene (total concentration, 28 mg mL^{-1} for PCDTBT : Et$_2$-*cis*-1-[70]PBC (1 : 3, w/w) and PCDTBT : Ph$_2$-*cis*-1-[70]PBC (1 : 3, w/w); 21 mg mL^{-1} for PCDTBT : Et$_2$-α-1-α-[70]PBC (1 : 2, w/w); 14 mg mL^{-1} for PCDTBT : Th$_2$-*cis*-1-[70]PBC (1 : 1, w/w); 35 mg mL^{-1} for PCDTBT : [70]PCBM (1 : 4, w/w) was prepared in ODCB and filtered with a 0.45 μm porous filter. The active layer was spin-coated (at 1500 rpm for 60 s for PCDTBT : Et$_2$-*cis*-1-[70]PBC, PCDTBT : Et$_2$-α-1-α-[70]PBC, PCDTBT : Th$_2$-*cis*-1-[70]PBC and PCDTBT : Ph$_2$-*cis*-1-[70]PBC; at 1000 rpm for 60 s for PCDTBT : [70]PCBM) on the top of the PEDOT:PSS layer and then dried at 70 °C for 1 h. For the fabrication of the buffer layer, a solution of titanium isopropoxide in ethanol was spin-coated at 4000 rpm for 20 s onto the ITO/PEDOT:PSS/PCDTBT : fullerene. The samples were dried in a desiccator at r.t. for 20 min, and finally transferred to an evaporation chamber for Al deposition (∼100 nm) before extracting their *J–V* characteristics under AM1.5 conditions.

The electron-only devices for the SCLC measurements were fabricated as follows. A 50 nm Al film was first thermally deposited onto the glass substrate. The PCDTBT : fullerene blend film with the same ratio as in the PSC device was spin-coated at 800 rpm. Then, the active layer was capped by a 100 nm Al electrode.

Solubility tests

The solubilities of fullerene derivatives were estimated as follows.[53] Saturated solutions of the fullerene materials were

prepared by adding an excess amount of the fullerenes to ODCB, followed by sonication at room temperature for 1 min. Then, the saturated solutions were filtered through a membrane filter (Cosmonice Filter S, COSMOSIL, pore size: 0.45 μm) to remove the aggregates. The amounts of the fullerene materials dissolved in the filtrates were determined by weighing the solid contents that remained after evaporation of the solvent and thorough drying under vacuum.

Conflicts of interest

There are no conflicts to declare.

Acknowledgements

References

1 T. Umeyama and H. Imahori, *J. Mater. Chem. A*, 2014, **2**, 11545.

2 K. A. Mazzio and C. K. Luscombe, *Chem. Soc. Rev.*, 2015, **44**, 78.

3 S. Xiao, Q. Zhang and W. You, *Adv. Mater.*, 2017, **29**, 1601391.

4 Y. Cai, L. Huo and Y. Sun, *Adv. Mater.*, 2017, **29**, 1605437.

5 R. Ganesamoorthy, G. Sathiyan and P. Sakthivel, *Sol. Energy Mater. Sol. Cells*, 2017, **161**, 102.

6 H. Imahori, *Bull. Chem. Soc. Jpn.*, 2007, **80**, 621.

7 C. B. Nielsen, S. Holliday, H.-Y. Chen, S. J. Cryer and I. McCulloch, *Acc. Chem. Res.*, 2015, **48**, 2803.

8 S. Li, Z. Zhang, M. Shi, C.-Z. Li and H. Chen, *Phys. Chem. Chem. Phys.*, 2017, **19**, 3440.

9 W. Zhao, S. Li, H. Yao, S. Zhang, Y. Zhang, B. Yang and J. Hou, *J. Am. Chem. Soc.*, 2017, **139**, 7148.

10 Z. Fei, F. Eisner, X. Jiao, M. Azzouzi, J. Röhr, Y. Han, M. Shahid, A. Chesman, C. Easton, C. McNeill, T. Anthopoulos, J. Nelson and M. Heeney, *Adv. Mater.*, 2018, **30**, 1705209.

11 M. M. Wienk, J. M. Kroon, W. J. H. Verhees, J. Knol, J. C. Hummelen, P. A. van Hal and R. A. J. Janssen, *Angew. Chem., Int. Ed.*, 2003, **42**, 3371.

12 Y. He, G. Zhao, B. Peng and Y. Li, *Adv. Funct. Mater.*, 2010, **20**, 3383.

13 Y. Li, *Chem.–Asian J.*, 2013, **8**, 2316.

14 M. Lenes, G.-J. A. H. Wetzelaer, F. B. Kooistra, S. C. Veenstra, J. C. Hummelen and P. W. M. Blom, *Adv. Mater.*, 2008, **20**, 2116.

15 Y. He, H.-Y. Chen, J. Hou and Y. Li, *J. Am. Chem. Soc.*, 2010, **132**, 1377.

16 M. R. Cerón, M. Izquierdo, A. Aghabali, A. J. Valdez, K. B. Ghiassi, M. M. Olmstead, A. L. Balch, F. Wudl and L. Echegoyen, *J. Am. Chem. Soc.*, 2015, **137**, 7502.

17 T. Umeyama, T. Miyata, A. C. Jakowetz, S. Shibata, K. Kurotobi, T. Higashino, T. Koganezawa, M. Tsujimoto, S. Gélinas, W. Matsuda, S. Seki, R. H. Friend and H. Imahori, *Chem. Sci.*, 2017, **8**, 181.

18 T. Umeyama, S. Shibata, K. Igarashi, S. Takahara, T. Higashino, S. Seki and H. Imahori, *Chem. Lett.*, 2017, **46**, 1001.

19 T. Umeyama, S. Shibata, T. Miyata, K. Igarashi, T. Koganezawa and H. Imahori, *RSC Adv.*, 2017, **7**, 45697.

20 T. Umeyama, K. Igarashi, D. Sakamaki, S. Seki and H. Imahori, *Chem. Commun.*, 2018, **54**, 405.

21 A. Herrmann, F. Diederich, C. Thilgen, H.-U. T. Meer and W. H. Müller, *Helv. Chim. Acta*, 1994, **77**, 1689.

22 N. Haruta, T. Sato and K. Tanaka, *J. Org. Chem.*, 2012, **77**, 9702.

23 S. Kitaura, K. Kurotobi, M. Sato, Y. Takano, T. Umeyama and H. Imahori, *Chem. Commun.*, 2012, **48**, 8550.

24 D. S. Sabirov, *J. Phys. Chem. C*, 2013, **117**, 9148.

25 X. Meng, G. Zhao, Q. Xu, Z. a. Tan, Z. Zhang, L. Jiang, C. Shu, C. Wang and Y. Li, *Adv. Funct. Mater.*, 2014, **24**, 158.

26 M.-H. Liao, Y.-Y. Lai, Y.-Y. Lai, Y.-T. Chen, C.-E. Tsai, W.-W. Liang and Y.-J. Cheng, *ACS Appl. Mater. Interfaces*, 2014, **6**, 996.

27 R. Tao, T. Umeyama, K. Kurotobi and H. Imahori, *ACS Appl. Mater. Interfaces*, 2014, **6**, 17313.

28 R. Tao, T. Umeyama, T. Higashino, T. Koganezawa and H. Imahori, *Chem. Commun.*, 2015, **51**, 8233.

29 B. Zhang, J. Subbiah, Y. Y. Lai, J. M. White, D. J. Jones and W. W. H. Wong, *Chem. Commun.*, 2015, **51**, 9837.

30 B. Zhang, J. M. White, D. J. Jones and W. W. H. Wong, *Org. Biomol. Chem.*, 2015, **13**, 10505.

31 D. S. Sabirov, A. O. Terentyev and R. G. Bulgakov, *J. Phys. Chem. C*, 2015, **119**, 10697.

32 F. Zhao, X. Meng, Y. Feng, Z. Jin, Q. Zhou, H. Li, L. Jiang, J. Wang, Y. Li and C. Wang, *J. Mater. Chem. A*, 2015, **3**, 14991.

33 Z. Xiao, X. Geng, D. He, X. Jia and L. Ding, *Energy Environ. Sci.*, 2016, **9**, 2114.

34 Z.-J. Li, S. Wang, S.-H. Li, T. Sun, W.-W. Yang, K. Shoyama, T. Nakagawa, I. Jeon, X. Yang, Y. Matsuo and X. Gao, *J. Org. Chem.*, 2017, **82**, 8676.

35 T. Cao, N. Chen, G. Liu, Y. Wan, J. D. Perea, Y. Xia, Z. Wang, B. Song, N. Li, X. Li, Y. Zhou, C. J. Brabec and Y. Li, *J. Mater. Chem. A*, 2017, **5**, 10206.

36 D. S. Sabirov, *J. Phys. Chem. C*, 2016, **120**, 24667.

37 W. W. H. Wong, J. Subbiah, J. M. White, H. Seyler, B. L. Zhang, D. J. Jones and A. B. Holmes, *Chem. Mater.*, 2014, **26**, 1686.

38 R. Tao, T. Umeyama, T. Higashino, T. Koganezawa and H. Imahori, *ACS Appl. Mater. Interfaces*, 2015, **7**, 16676.

39 L.-L. Deng, X. Li, S. Wang, W.-P. Wu, S.-M. Dai, C.-B. Tian, Y. Zhao, S.-Y. Xie, R.-B. Huang and L.-S. Zheng, *Sci. Bull.*, 2016, **61**, 132.

40 We follow the nomenclature for [70]fullerene bis-adducts proposed by Echegoyen, *et al.* in ref. 16. In this rule, Greek

letters such as α, β, γ, and δ define the reacted [6,6]-bonds, and numbers represent the smallest number of bonds separating the addition sites. The same type of bonds on opposite semisphere across the δ-bonds are differentiated using a prime designation. In addition, we also apply the nomenclature of [60]fullerene bis-adducts to [70]fullerene ones; "cis-1" means that two addends exist at [6,6]-bonds in the same hexagon (e.g., α-1-α and α-1-β), and "cis-2" that two addends exist at [6,6]-bonds in the hexagons next to each other (e.g., α-2-α) (Fig. 1b).

41 M. R. Cerón and L. Echegoyen, *J. Phys. Org. Chem.*, 2016, **29**, 613.

42 S. Beaupré and M. Leclerc, *J. Mater. Chem. A*, 2013, **1**, 11097.

43 T. Umeyama, Y. Watanabe, E. Douvogianni and H. Imahori, *J. Phys. Chem. C*, 2013, **117**, 21148.

44 B. M. Savoie, A. Rao, A. A. Bakulin, S. Gelinas, B. Movaghar, R. H. Friend, T. J. Marks and M. A. Ratner, *J. Am. Chem. Soc.*, 2014, **136**, 2876.

45 S. Shoaee, S. Subramaniyan, H. Xin, C. Keiderling, P. S. Tuladhar, F. Jamieson, S. A. Jenekhe and J. R. Durrant, *Adv. Funct. Mater.*, 2013, **23**, 3286.

46 L. S. Barreto, O. L. Alves and R. A. Jackson, *Phys. Chem. Glasses*, 2002, **43C**, 119.

47 The ratio of α-1-α : α-1-β in Ph$_2$-*cis*-1-[70]PBC was reported to be 78 : 22 in ref. 16, whereas 68 : 32 in Ph$_2$-*cis*-1-[70]PBC obtained in this study. The slight difference in the composition ratio may result from the difference in the analysis method; the isolation yields were calculated after preparative thin layer chromatography in ref. 16, while peak area ratios in HPLC traces were used in this study.

48 We tried to obtain X-ray single crystal structure of Et$_2$-α-1-α-[70]PBC, but sufficiently large single crystal for the measurement was not obtained.

49 C. Cardellicchio, V. Fiandanese, G. Marchese and L. Ronzini, *Tetrahedron Lett.*, 1987, **28**, 2053.

50 R. Doi, M. Shibuya, T. Murayama, Y. Yamamoto and Y. Iwabuchi, *J. Org. Chem.*, 2015, **80**, 401.

51 D. C. Owsley, J. M. Nelke and J. J. Bloomfield, *J. Org. Chem.*, 1973, **38**, 901.

52 M. J. Frisch, G. W. Trucks, H. B. Schlegel, G. E. Scuseria, M. A. Robb, J. R. Cheeseman, G. Scalmani, V. Barone, B. Mennucci, G. A. Petersson, H. Nakatsuji, M. Caricato, X. Li, H. P. Hratchian, A. F. Izmaylov, J. Bloino, G. Zheng, J. L. Sonnenberg, M. Hada, M. Ehara, K. Toyota, R. Fukuda, J. Hasegawa, M. Ishida, T. Nakajima, Y. Honda, O. Kitao, H. Nakai, T. Vreven, J. A. Montgomery, Jr., J. E. Peralta, F. Ogliaro, M. Bearpark, J. J. Heyd, E. Brothers, K. N. Kudin, V. N. Staroverov, R. Kobayashi, J. Normand, K. Raghavachari, A. Rendell, J. C. Burant, S. S. Iyengar, J. Tomasi, M. Cossi, N. Rega, J. M. Millam, M. Klene, J. E. Knox, J. B. Cross, V. Bakken, C. Adamo, J. Jaramillo, R. Gomperts, R. E. Stratmann, O. Yazyev, A. J. Austin, R. Cammi, C. Pomelli, J. W. Ochterski, R. L. Martin, K. Morokuma, V. G. Zakrzewski, G. A. Voth, P. Salvador, J. J. Dannenberg, S. Dapprich, A. D. Daniels, Ö. Farkas, J. B. Foresman, J. V. Ortiz, J. Cioslowski and D. J. Fox, *Gaussian 09*, Gaussian, Inc., Wallingford CT, 2009.

53 T. Umeyama, S. Shibata and H. Imahori, *RSC Adv.*, 2016, **6**, 83758.